Calibration and Quality Assurance of an Airborne Turbulence Probe in an Aeronautical Wind Tunnel

RONALD DOBOSY, EDWARD J. DUMAS, AND DAVID L. SENN

Atmospheric Turbulence and Diffusion Division, NOAA/ARL, and Oak Ridge Associated Universities, Oak Ridge, Tennessee

BRUCE BAKER

Atmospheric Turbulence and Diffusion Division, NOAA/ARL, Oak Ridge, Tennessee

DAVID S. SAYRES AND MARK F. WITINSKI

School of Engineering and Applied Sciences, Harvard University, Cambridge, Massachusetts

CLAIRE HEALY AND JASON MUNSTER

Department of Earth and Planetary Sciences, Harvard University, Cambridge, Massachusetts

JAMES G. ANDERSON

School of Engineering and Applied Sciences, Harvard University, Cambridge, Massachusetts

(Manuscript received 14 November 2011, in final form 17 September 2012)

ABSTRACT

The Best Aircraft Turbulence (BAT) probe is used by multiple research groups worldwide. To promote an accurate interpretation of the data obtained from the probe's unusual nine-port design, a detailed understanding of the BAT probe's function along with a characterization and minimization of its systematic anomalies is necessary. This paper describes recent tests to enhance understanding of the probe's behavior. The tests completed in the Wright Brothers Wind Tunnel at the Massachusetts Institute of Technology (MIT) built on earlier findings at Purdue University. Overall the true-vertical wind relative to the probe was found to have a systematic anomaly of about 10%–15%, an acceptable value borne out by considerable field experience and further reducible by modeling and removing. However, significant departure from theoretical behavior was found, making detailed generalization to other BAT probes still inadvisable. Based on these discoveries, recommendations are made for further experiments to explain the anomalous behavior, reduce the systematic anomaly, and generalize the characterizations.

1. Introduction

The Best Aircraft Turbulence (BAT) probe was developed explicitly for environmental research from small aircraft (Crawford and Dobosy 1992, hereafter CD92). The pressure distribution over a sphere had been found among multiple alternatives to be the most effective measure of flow relative to an airplane (Brown et al. 1983). Major research centers developed airborne systems capable of accurate turbulence measurements (Lenschow 1986; MacPherson et al. 1992; LeMone et al. 2003), but these required large aircraft and expensive instruments. The BAT probe's innovation was to use the newly available small pressure sensors and accelerometers along with the global positioning system (Crawford and Dobosy 1997). This allowed motion of the wind relative to the probe and of the probe relative to earth to be measured all in one small package. The result was lightweight, inexpensive, self-contained, and undemanding of power. With the BAT probe it became possible for a small research organization to make airborne turbulence measurements.

Corresponding author address: R. J. Dobosy, Atmospheric Turbulence and Diffusion Division, NOAA/ARL, Oak Ridge, TN 37830.
E-mail: ron.dobosy@noaa.gov

DOI: 10.1175/JTECH-D-11-00206.1

A second generation of the BAT probe was developed in collaboration with Airborne Research Australia (Hacker and Crawford 1999). Three of these probes were fitted to a slow-flying, high-altitude airplane used to investigate turbulence-induced refraction of electromagnetic waves, radio and visible, in the upper troposphere (Wroblewski et al. 2007).

Around 1998, *Initiative Industriali Italiane* applied the BAT probe to a small (650 kg) single-engine two-place airplane of their manufacture to provide the commercially available Sky Arrow 650 environmental research airplane (ERA). A Sky Arrow of this type was acquired by San Diego State University for their work in Alaska (Zulueta et al. 2011). Groups in Italy, Sweden, and the Netherlands use the airplane (Gioli et al. 2004, 2006; Vellinga et al. 2010), as does the University of Alabama (Hall et al. 2006; Kirby et al. 2008). Other groups have independently developed similar systems (Neininger et al. 2001; Bange et al. 2007; van den Kroonenberg et al. 2008; Beswick et al. 2008; Avissar et al. 2009).

Such instruments may receive limited wind tunnel testing during their development (e.g., CD92), but rarely in a fully adequate wind tunnel. An exception is van den Kroonenberg et al. (2008), but they use a different design. The work at Purdue University (Garman et al. 2006) provided the BAT probe's first real test. This test revealed asymmetry in the derived angle of attack that was not evident in the angle of sideslip. The only observed source of asymmetry was the fast ultrasensitive temperature sensor (FUST), described by French et al. (2001). A small downward-protruding obstruction, it was 90° in angular separation from the central port. Nevertheless, this small asymmetry evidently caused important departure from ideal behavior. Based on this discovery, Garman et al. (2006) recommended wind tunnel testing for each individual probe.

Because of the logistical difficulty of accessing an appropriate wind tunnel, however, most turbulence probes are calibrated only in flight (Lenschow 1986; Bögel and Baumann 1991; Kalogiros and Wang 2002). Such in-flight calibrations account adequately for departures from ideal behavior as is evident in the match between airborne and tower-mounted flux measurements (Crawford et al. 1996b; Crawford and Dobosy 2004; Kirby et al. 2008; Zulueta et al. 2011; Vellinga et al. 2013). The critical advantage of a wind tunnel is the full control over both airspeed and incidence angle on the probe. In flight, generating lift distorts the flow (Crawford et al. 1996a; Garman et al. 2008) and ties the incidence angle to the airspeed.

In this paper we describe wind tunnel tests on a BAT probe, resulting from a collaboration between National Oceanic and Atmospheric Administration (NOAA)/ATDD and the Anderson Group at Harvard University. The Anderson Group has developed a sophisticated gas analyzer of atmospheric CO_2, H_2O, CH_4, and their isotopologues using integrated cavity output spectroscopy (ICOS; Sayres et al. 2009; Witinski et al. 2011). This instrument is small enough to fly on a light twin-engine airplane and has a sample rate sufficient for eddy correlation, at least for the most common isotopologues. Paired with the BAT probe, the system can measure the fluxes of trace gases to assess, among other things, changes in Arctic sources of CH_4.

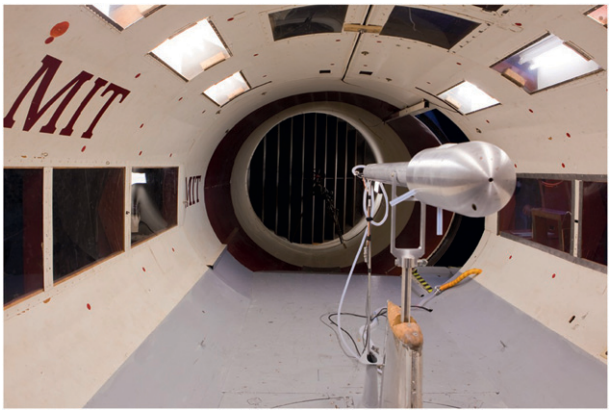

FIG. 1. BAT probe in Wright Brothers Wind Tunnel. The Harvard ICOS gas analyzers' three plastic inlet tubes (13-mm diameter, two visible) extend 70 mm radially from the lower quadrant 250 mm behind the probe's head.

Tests were recently run at the Massachusetts Institute of Technology (MIT) in the Wright Brothers Wind Tunnel (WBWT), an aeronautical tunnel of sufficient size and power to enable full-speed tests of the BAT probe over a full matrix of incident angles (see Fig. 1). These tests extend the work of Garman et al. (2006) and address remaining questions as to the functioning of the BAT probe, while at the same time characterizing in detail the particular probe to be used in the upcoming Arctic flux missions.

2. BAT probe description

The BAT probe (Fig. 2) consists of a 155-mm hemisphere with ports arranged to measure the pressure distribution over its surface. It protrudes into relatively undisturbed air forward of the airplane to measure the flow speed and direction incident on its sensor head. This vector plus the probe's velocity over the ground, supplied by global positioning and inertial navigation systems (GPS/INS), yields wind and turbulence relative to the earth. Covariance with high-sample-rate measurements of

trace gases and temperature yields turbulent fluxes (e.g., Crawford et al. 1996b).

All pressure sensors are micromachined silicon and fit within the probe's head minimizing the length of their lines. The hemisphere mates to a cylinder 222.2 mm long, followed by a taper to 82.6 mm in diameter to couple to a boom protruding from the airplane's nose. The head of the probe is machined from 6061-T6 aluminum. The probe's central port p_0 is 7.94 mm in diameter. Eight additional ports, 1.02 mm in diameter, are equally distributed around the circumference of a circle separated from p_0 by 45°. Four ports $p_{r1\ldots r4}$ link to a common junction through flexible silicone plastic tubes of 1.59-mm diameter and 96- ± 1.6-mm length. By Hagen–Poiseuille theory the pressure at this junction is the average of the pressures at the four ports $\overline{p_r}$. This absolute reference is roughly the static (i.e., ambient) pressure.

The incident flow's dynamic pressure q is determined from the pressure difference $\delta_x p$, essentially a Pitot-static system. A weak bypass flow in port p_0, originally intended to ventilate a high-rate temperature sensor, reduces $\delta_x p$ by about 2% (CD92). The difference is treated by calibration (section 7). The incident flow's direction is given by an angle of attack α and an angle of sideslip β. These angles, optimized for high-accuracy environmental wind measurement rather than flight dynamics, do not conform to ISO-1151 (International Organization for Standardization 1988; see Fig. 5). The angle of attack α comes from $\delta_z p$, defined in Fig. 2 and section 4. The angle of sideslip β comes from $\delta_y p$.

Drawing on the observations of Garman et al. (2006), the FUST probe is mounted 100 mm behind the hemisphere. This BAT probe also has a fast-flow port containing a microbead thermistor for use absent the FUST. This port feeds a cylindrical conduit 6.35 mm in diameter inclined at an angle of 27° to the horizontal, and 30° to the long axis of the probe (Fig. 2). Although this port may appear from the figure to affect the pressure at port p_4, hence $\delta_z p$, there was little distortion evident in the field of $\delta_z p$ (section 6a).

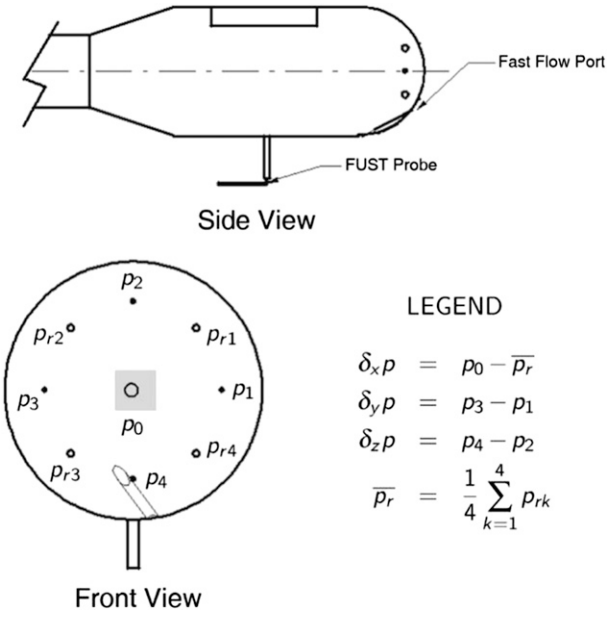

FIG. 2. BAT probe schematic. Pressure ports $p_{1\ldots4}$ determine the direction and speed of the incoming airflow with p_0 providing, roughly, the Pitot (total) pressure. The average pressure $\overline{p_r}$ over $p_{r1\ldots r4}$ provides the absolute reference, roughly the static (ambient) pressure (see text and section 4). The square about p_0 depicts the range of incident flow directions used in the wind tunnel tests. In flight, the stagnation point falls within this area.

3. Wright Brothers Wind Tunnel description

The WBWT is ideal for a test of the BAT probe. It has a closed-return, continuous flow with a test section 4.5 m long having elliptical cross section with axes 3 and 2.25 m. Its flow speed can exceed the planned flight speed of 62 m s^{-1} avoiding uncertainty because of the limited test-section area (CD92) or slower flow than in actual flight (Garman et al. 2006).

The standard mount for test objects in the WBWT has a range of ±20° in pitch angle θ and ±10° in yaw angle ψ (Fig. 3). Yaw and pitch can be adjusted remotely without halting the flow. Pressures and temperature were collected from the wind tunnel at 2 s^{-1}, and from the BAT probe at 50 s^{-1}.

The BAT probe is specified to report α and β to higher precision than available from the normal ψ and θ measurements at the WBWT, requiring supplemental instruments. To determine ψ we measured distance Y of Fig. 3 using a laser rangefinder (Leica Disto) mounted on the sidewall of the test section. This measurement was manually read at each new ψ setting. A Spi-Tronic Pro 3600 digital level mounted on the aft end of the probe's boom reported θ via an RS-232 serial interface at 2 s^{-1}. Its uncertainty is 0.01° between ±10° and 0.1° otherwise.

Figure 4 (Covert 2004) shows the flow-direction anomalies in the clean tunnel looking downstream at a cross section near the center of rotation. (Figs. 3 and 5). The wind speed is 46.5 m s^{-1}. The dynamic pressure anomalies, also presented by Covert (2004), are within 1%, considered negligible (see section 7).

4. Mathematical background

The BAT probe determines the direction and speed of the incident flow from the distribution of pressure

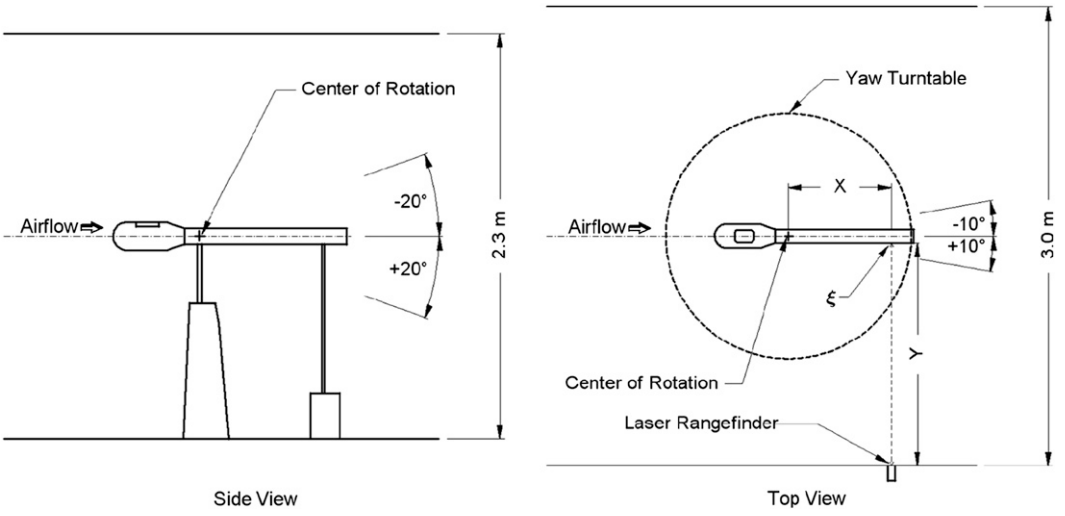

FIG. 3. Schematic of measurement and control of (left) pitch θ and (right) yaw ψ in the MIT wind tunnel. Note that both ψ and θ are positive clockwise. With the probe level, the laser precisely measures Y from which the angle ξ is found. Adding the appropriate offset yields ψ. An electronic level directly measures θ.

produced over its hemispherical head. Hence processing of its measurements assumed a spherical geometry. Noting the probe's actual shape, however, a reviewer of this paper mentioned work with hemisphere-cylinder (H-C) heads. As long as the stagnation point remains within ±15° of the central port the pressure pattern closely matches that over a sphere apart from a parameter adjustment (Traub and Rediniotis 2003). In flow at ambient pressure p and dynamic pressure q at angle ζ from the stagnation point:

$$p_\zeta = p + q(1 - k_p \sin^2\zeta). \tag{1}$$

For a sphere $k_p = 9/4$. For a H-C $k_p = 2.07$, determined empirically. The pattern also applies to fully turbulent flow out to about 60° from the stagnation point. In coordinated flight the stagnation point remains within ±10°, and the most remote port does not exceed 55° from the stagnation point even in strong turbulence.

To facilitate calculation of α and β, use quantities E_α and E_β, which approximate α and β when these angles are small:

$$E_\alpha = K_\alpha \frac{\delta_z p}{q_\star},$$

$$E_\beta = K_\beta \frac{\delta_y p}{q_\star}, \tag{2}$$

with $\delta_y p$ and $\delta_z p$ defined in Fig. 2. The $q_\star$ is nominally the dynamic pressure q. Its actual value depends on the processing scheme.

Two processing schemes are relevant to computing α and β, and if not already known, q. The "BAT" scheme of Eckman (1999) explicitly uses measurements made on the BAT probe, setting $q_\star = \delta_x p$ in (2). The "low resolution" scheme of Rosemount, described by J. A. Leise and J. M. Masters (1993, unpublished manuscript), obtains q independently of the probe, usually from the airplane's Pitot-static system, and sets $q_\star = q$ directly. Both schemes also provide the ambient pressure p and (beyond this paper's scope) the ambient temperature T.

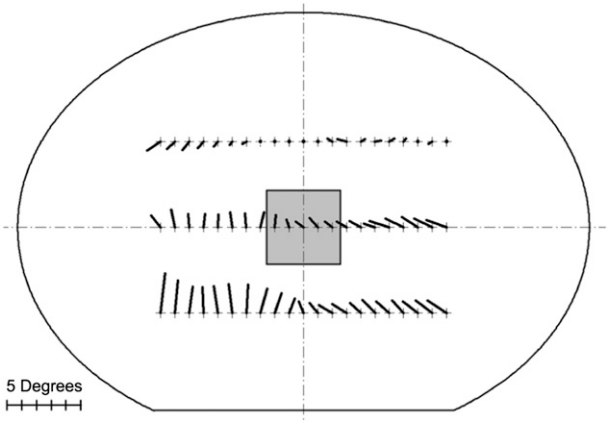

FIG. 4. Cross section of flow-direction anomalies looking downstream in the clean WBWT. The scale, given in the lower-left corner, is greatly amplified for clarity. The vertical (horizontal) component is α (β). The central square depicts the range of BAT probe positions. Within this range, the maximum anomaly is 1°.

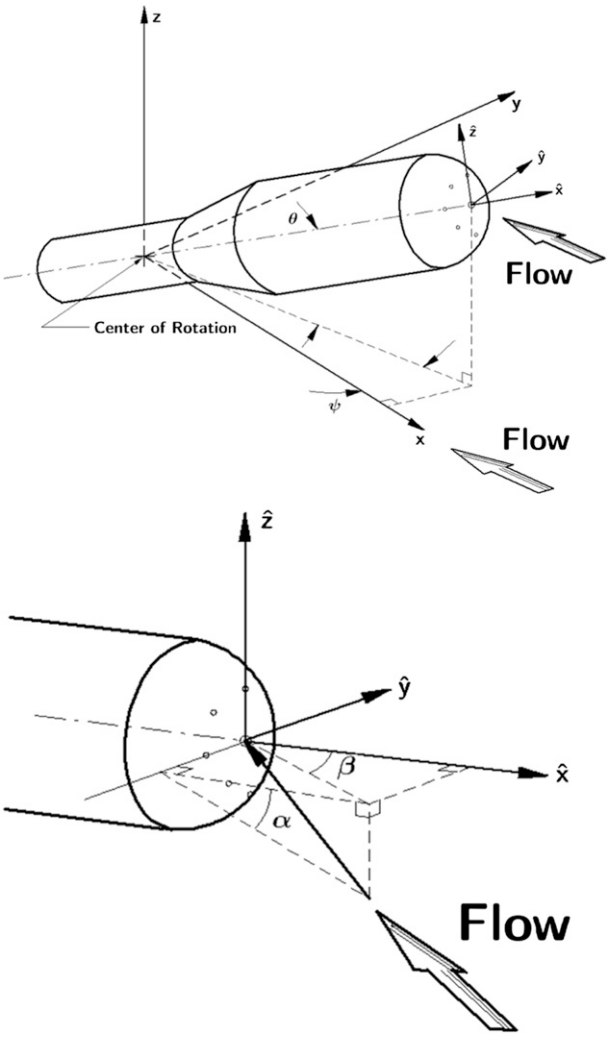

FIG. 5. (top) Schematic of Cartesian coordinates for the wind tunnel (unadorned) and the probe (hat). Attitude angles ψ and θ are set as azimuth and elevation (spherical polar coordinates) on the wind tunnel's mount, but are also yaw and pitch if roll remains zero. (bottom) Incidence angles β and α, positive as depicted. These are objects in the probe's rectangular Cartesian coordinates, directly related to the $\hat{\mathbf{j}}$ and $\hat{\mathbf{k}}$ components of the incident flow; see (12). These conventions of airborne environmental-wind measurement notably do not match ISO-1151 (International Organization for Standardization 1988).

The BAT scheme's use of $q_\star = \delta_x p$ makes K_α and K_β specific to the angle ϕ_r from each diagonal port $p_{r1\ldots r4}$ to p_0. This is seen in Fig. 2 where $\delta_x p$ depends on $\overline{p_r}$. On the BAT probe, ϕ_r is 45°. The low-resolution scheme making no use of $\delta_x p$ does not require the additional four ports $p_{r1\ldots r4}$.

The BAT scheme's K_α and K_β are independent of k_p. Because of (1), k_p is a common factor in all of $\delta_x p$, $\delta_y p$, and $\delta_z p$ and divides out of (2). The low-resolution scheme, not deriving q from $\delta_x p$, has K_α and K_β inversely proportional to k_p.

TABLE 1. Parameters and coefficients given by theory for BAT and low-resolution schemes.

Parameter	BAT ($\phi_r = 45°$)	Low resolution (ϕ_r irrelevant)
K_α, K_β	0.250	0.242
$q_\star$	$\delta_x p$	q
K_r	2	−4

Computation of β and α by either scheme proceeds:

$$S\tan\beta = 2E_\beta,$$
$$S\tan\alpha = 2E_\alpha,$$
$$S = 1 + \sqrt{1 + K_r(E_\beta^2 + E_\alpha^2)}. \qquad (3)$$

Table 1 gives K_α, K_β, $q_\star$, and K_r for the two schemes.[1]

Knowing α and β, one can compute q (BAT scheme) and p. For the BAT scheme (with $\phi_r = 45°$), the expression for q is

$$q = \frac{4\delta_x p}{k_p}\left[\frac{1 + \tan^2\beta + \tan^2\alpha}{2 - \tan^2\beta - \tan^2\alpha}\right]. \qquad (4)$$

In the low-resolution scheme, q is an input parameter.

The ambient pressure is given by:

$$p = p_r + \frac{q}{4}\left[k_p\frac{2 + \tan^2\beta + \tan^2\alpha}{1 + \tan^2\beta + \tan^2\alpha} + 4(1 - k_p)\right]. \qquad (5)$$

In head-on flow to a sphere, when $(\alpha, \beta) = (0, 0)$, $\overline{p_r}$ is theoretically equal to ambient pressure given $\phi_r = 41.81°$. The BAT probe, however, uses $\phi_r = 45°$ based on early wind tunnel tests (CD92). Interestingly, for a H-C the corresponding value is $\phi_r = 44.0°$.

5. Calibration standards: Flow speed and incidence angles

In the wind tunnel's coordinates, (x, y, z) of Fig. 5, the flow is represented as $\mathbf{V} = [-U, 0, 0]$ with the speed U known independent of the BAT probe. Viewed from the probe in $(\hat{x}, \hat{y}, \hat{z})$ coordinates, $\mathbf{V}$ has three nonzero components $(A\hat{\mathbf{i}} + B\hat{\mathbf{j}} + C\hat{\mathbf{k}})U$, where A, B, and C are functions of the ψ and θ at which the mount is set. The two coordinate systems' difference in origin is inconsequential since the probe's head never leaves the region of uniform flow, apart from the irregularities shown in Fig. 4. The true angles of incidence, set β and set α (Fig. 5, lower), can be known independent of the probe's measurements through ψ and θ using relations

[1] For the "BAT" scheme with the BAT probe's port configuration, Eckman's implied K_β, K_α are both 0.125, half the K_β, K_α of Table 1. Thus, his $(H_y, H_z) = 0.5(E_\beta, E_\alpha)$ hence his larger constants in (3).

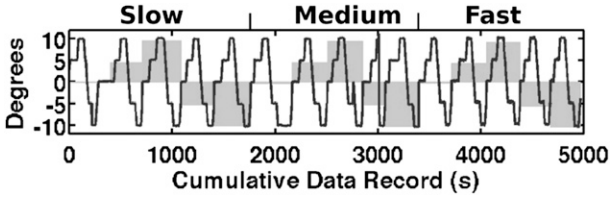

FIG. 6. Time series of set pitch angle θ (black curve) and set yaw angle ψ (gray shading) over the course of the wind tunnel test. At least 30 s were taken at each of the 75 pitch-angle settings.

given by J. A. Leise and J. M. Masters (1993, unpublished manuscript). They use Cartesian coordinates rather than the less elegant polar coordinate form of CD92. The resulting relations are gratifyingly simple:

$$\beta = -\psi,$$
$$\tan\alpha = \frac{\tan\theta}{\cos\psi}, \tag{6}$$

but applying them requires alignment.

By (6), the true zeros of ψ and θ correspond to the probe's reported zeros of β and α, hence to the zeros of $\delta_y p$ and $\delta_z p$. Precise alignment between probe and flow especially in ψ required a differential technique. First, the probe was carefully leveled in both pitch and roll by electronic level. Since the mount allowed no roll the $\delta_y p$-ports remained horizontal throughout the run. A preliminary alignment for ψ was set approximately by eye and measured precisely by laser rangefinder to establish the azimuthal reference point. The test then filled a 25-point matrix from nominally $-10°$ to $+10°$ in 5° steps for each of θ and ψ in three wind speed classes: slow, medium, and fast: (36, 51, and 61 m s^{-1}, respectively) (Fig. 6). The slow class applies to the Sky Arrow, the medium to our original implementation (CD92), and the fast to the current Harvard collaboration. At least 30 s were taken at each setting. The electronic level reported θ relative to horizontal at 2 s^{-1} while we measured the relative ψ by laser at each new setting. The offset between the preliminary (raw) settings and the true set values β_S and α_S was determined in postprocessing (slow, medium, fast):

$$\beta_s = \beta_{\text{raw}} - (0.83°, 0.42°, 1.03°) \quad \text{and}$$
$$\alpha_s = \alpha_{\text{raw}} - (0.43°, 0.19°, 0.64°).$$

An analogous situation exists in flight, where GPS/INS is rarely aligned exactly with the flowstream.

6. Results

Figures 7–9 are contour plots over the range of incidence angles tested. They map onto the small gray square on the face of the probe in Fig. 2 with the central port at (0, 0) of α_S and β_S. The square is not centered on p_0 because of the offsets, especially in β_S. The small crosses of Figs. 7–9 mark the 25 set angles (β_S, α_S) at which the data were taken. The inverted sign convention follows (12) and Fig. 5 bottom panel.

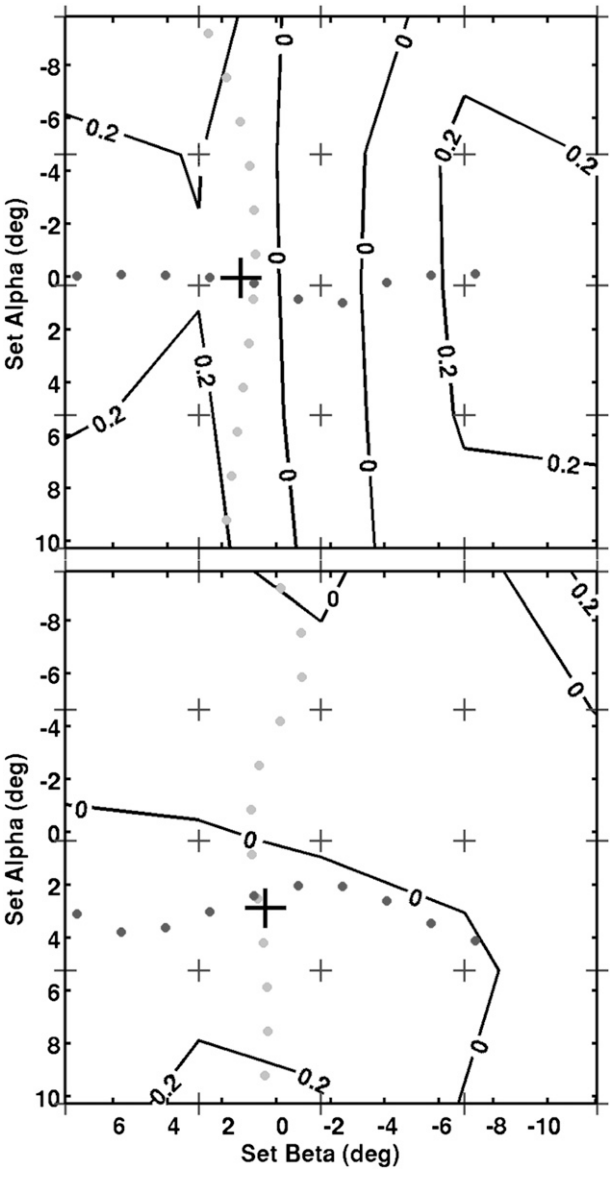

FIG. 7. Anomolies of (top) $\delta_y p$ and (bottom) $\delta_z p$, expressed as equivalent α and β (degrees) at the fast speed. Small crosses mark the data points. Port p_0 is at (0, 0). See Figs. 2 and 5 and text for details.

The large cross marks the center of ''mass'' of the rectangular subregion centered on (0, 0) and delineated by the range of the dots. The dots along each line mark the centers of ''mass'' along slices taken perpendicular to that line. ''Mass'' density is defined as the local value

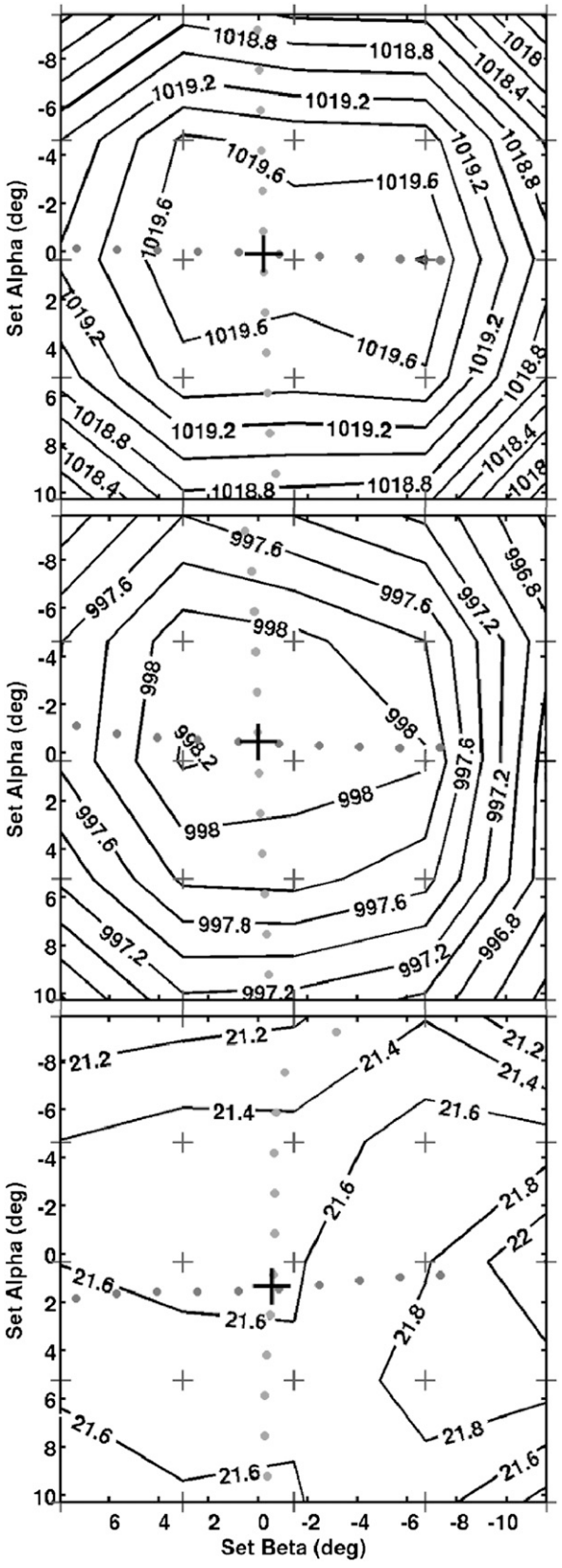

FIG. 8. Isobars (hPa) of (top) temperature-independent p_0, (middle) $\overline{p_r}$, and (bottom) $\delta_x p$ at the fast speed. See text for details and Fig. 2 for definitions.

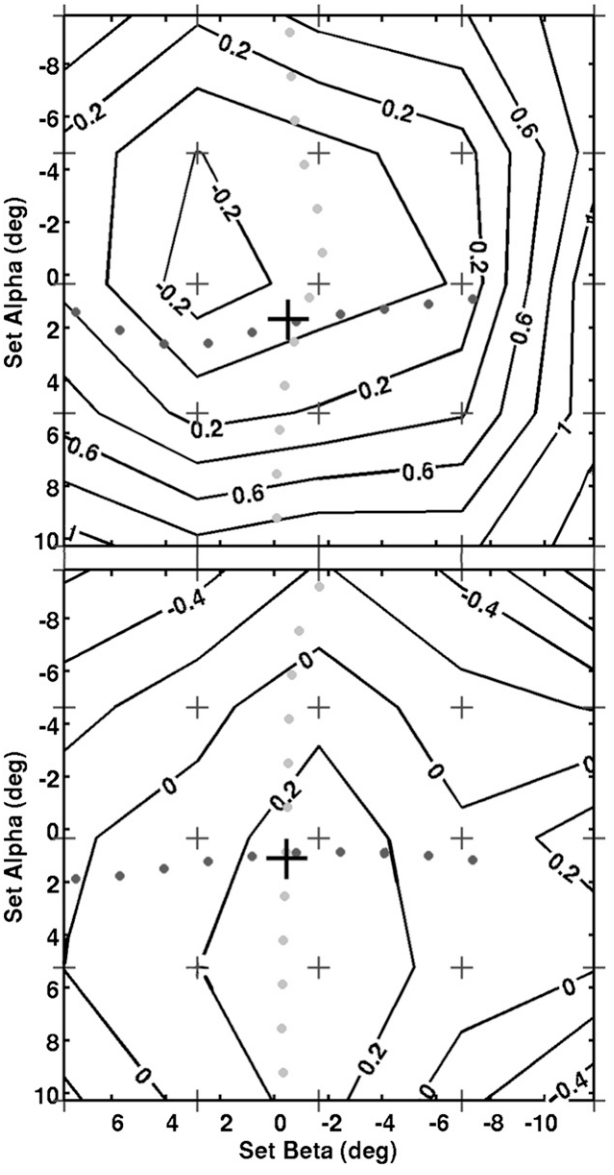

FIG. 9. (top) Discrepancy (hPa) between temperature-independent forms of dynamic pressure q estimated by (4) and q measured by the wind tunnel for the fast speed. (bottom) As in (top), but using $\delta_x p$ instead of (4) to estimate q.

of the plotted quantity minus the overall algebraic minimum value over the analyzed subregion. The minimum mass density is thus always zero. These figures' sides will be identified as starboard and port, not right and left, because work with these probes, as with aircraft, requires addressing unambiguously the same physical locations looking both forward and aftward. These plots represent *aftward* views, hence port is to the right, the reverse of the usual mnemonic association. Different meanings of the word ''port'' (port side versus pressure port) will be made clear by context.

During the 3-h run, the temperature increased from 18° to 42°C. The static pressure in the wind tunnel remained constant with rising temperature but changed with speed class. With constant pressure and flow speed but rising temperature, dynamic pressure decreases. Significant warming occurred over the hour needed to complete the 25-point pattern depicted in Figs. 7–9, the lowest temperature being associated with the central data point and the highest with the figures' upper-right (i.e., port side) corner. This follows the protocol of the previous section (Fig. 6). The warming requires quantities dependent on q to be plotted in temperature-independent forms to avoid warping the figures. Affected are p_0, $\overline{p_r}$, $\delta_x p$, $\delta_y p$, $\delta_z p$, and the WBWT's q. Quantities proportional to q can be treated for each speed class analogously to the quantity q_{Ti}:

$$q_{Ti} = \frac{1}{2}\frac{p}{R\overline{T}}U^2 = q\,\frac{T}{\overline{T}}, \tag{7}$$

where $\overline{T}$ is the average temperature for the speed class. Although $\overline{p_r}$ and p_0 are not proportional to q, (7) does apply to $\overline{p_r} - p$ by (5), using the WBWT's mean p for each speed class. Then, $p_0 = \overline{p_r} + \delta_x p$.

a. Patterns of directly measured fields

Of the directly measured quantities, the most regular and symmetrical are the pressure differences $\delta_y p$ and $\delta_z p$. Figure 7 shows the pattern of their departure from β_S and α_S after conversion to equivalent β and α, respectively, through the low-resolution form of (3) with q taken from the WBWT. They were visually optimized by adjusting K_β and K_α as in section 7. At the fast speed, 0.2° represents an anomaly of 0.2 m s^{-1}. Ideally, the patterns are flat. A few weak anomalies appear away from the center, more so in the lateral ($\delta_y p$) than the vertical.

The pressure p_0 (Fig. 8, top) is the sum of two direct measurements, $\overline{p_r}$ and $\delta_x p$. The overall pattern is symmetrical about the zeros of β_S and α_S although some asymmetry appears on the port side.

The absolute reference pressure $\overline{p_r}$ in Fig. 8 middle also shows symmetry with some departure to port. The differential $\delta_x p$ in Fig. 8 bottom panel has a more complex pattern, clearly asymmetrical on the far port side but of low relief. The maximum $\delta_x p$ is at the port edge of the measured array at $\beta_S = -10°$ and $\alpha_S = 0°$. Recall that the port edge of the pattern is farther from the central pressure port (larger $|\beta|$) than the starboard edge.

Although both $\overline{p_r}$ and $\delta_x p$ are direct measurements, they measure a weighted resultant of multiple physical inputs. These include the tube network interconnecting the four reference ports, the large central port, the small bypass (slow-flow port) in the central port's cavity, and the fast-flow port. Originally, the tubing network was the suspected source of the anomaly. This network, however, was found to have insignificant influence if properly installed and maintained (R. J. Dobosy et al. 2012, unpublished manuscript). Partial account for the remaining anomalies in $\overline{p_r}$ and $\delta_x p$ relative to the theory of section 4 is given in section 7.

b. Derived quantities p and q

Despite the insensitivity of $\delta_x p$ to α and β, the ambient absolute pressure p appears best represented by the theoretical expression (5) by virtue of the pattern's being closer to flat. The patterns are not displayed because the noise in the wind tunnel's reported static pressure [$\pm$15 hPa (1000 hPa)$^{-1}$] was sufficient to obliterate any actual variations in ambient pressure with which to test the probe's p. The wind tunnel did report significant static-pressure change with speed class, however. The p reported by the BAT probe was therefore compared with the mean static pressure reported by the wind tunnel for each speed class revealing a ~6-hPa offset the source of which has not yet been found. This 0.6% offset is considered negligible (see Table 2).

The low relief of $\delta_x p$ becomes obvious, however, in the departure of dynamic pressure computed using (4) from that given by the wind tunnel. Figure 9 top panel, which should be flat, shows a strong pattern of discrepancy. The $\delta_x p$ by itself yields much closer match. In Fig. 9 bottom panel, the anomaly varies about 60 Pa over most of the pattern. The upper figure shows anomalies near 100 Pa over the same region. Similar results are also found for the other speed classes.

For reasons currently unknown, this BAT probe behaves with regard to q more like a normal Pitot-static system than the theory predicts. Thus, dynamic pressure q is better represented by $\delta_x p$ itself with no adjustment for incident-flow angle. Nevertheless, the pattern of mean $\delta_x p$ displays significant departure from flat. Its value is smallest at the four corners of the pattern, qualitatively following theory.

7. Optimizations departing from strict theory

Accepting $\delta_x p$ as q makes the low-resolution scheme of Rosemount applicable since q is then known independent of α and β. Furthermore, α and β can be optimized by adjusting K_α and K_β. Likewise, one can provide for optimization of q by defining $q = \epsilon_q \delta_x p$, where $\epsilon_q = 1 \pm \epsilon$ and $0 < \epsilon \ll 1$. Special maneuvers to do this in flight are standard operational practice (Lenschow 1970; Bögel and Baumann 1991; Kalogiros and Wang 2002; Vellinga et al. 2013).

In a wind tunnel, such optimizations are more effective. Wind tunnel flow is free of flight-related flow distortions, especially upwash, and can cover the full range of speed and incidence direction unlimited by flight requirements. Clean-tunnel flow distortion in the WBWT was taken from measurements presented by Covert (2004). Direction distortion, interpolated over the square in Fig. 4 was accounted by adjusting α_S and β_S to improve the accuracy of these references. The speed distortion was within 1%, considered small relative to the anomalies in Table 2. The BAT probe's presence blocked less than 3% of the cross section, hence producing no sidewall effects or other distortions beyond those we sought to measure (e.g., Traub and Rediniotis 2003).

The optimum K_α was 0.21, 0.21, and 0.22 for the fast-, medium-, and slow-speed classes respectively. The corresponding optimum K_β was 0.225, 0.23, and 0.23. The ϵ_q was 0.99, 1.0, and 0.985.

a. Characteristics of derived α and β

The $\delta_z p$ and $\delta_y p$ from which the incidence angles α and β are derived have remarkably regular patterns with changing attitude in the tests. The pattern of q, however, introduces some irregularity. In the corners, the reported incidence angles are larger than the true angles because of the tendency of reported $\delta_x p$ to depart from q toward its theoretical pattern, as noted previously. In fact, through the maximum of $\delta_x p$ along the port edge, the pure, nonoptimized, theoretical BAT scheme produces an excellent match between the derived α and set α_S.

b. Mix of BAT and low-resolution schemes

The β reported by the BAT probe using the BAT-scheme version of (2) and (3) with optimized K_α and K_β varies by no more than $\pm 0.1°$ with changes in α_S at constant β_S. The probe's reported α, however, varies by as much as 3 times that much with changes in β_S at constant α_S. Using the low-resolution scheme with appropriately optimized K_α and K_β produces the reverse. A mix of the two schemes—β by BAT scheme and α by low-resolution scheme—appears to produce better accuracy than either scheme alone. Further analysis in this paper uses this mixed scheme.

8. Anomaly estimates

Eddy covariance for the vertical flux of scalars combines measurements of both concentration and vertical wind. The concentration is measured by such instruments as the ICOS gas analyzer noted in the introduction. The vertical wind is determined from the airflow relative to a wind sensor (e.g., BAT probe) and that sensor's motion, given by GPS/INS, relative to the earth. The focus of this paper, the wind probe, measures the incidence angles, α and β, and the dynamic pressure q. Anomalies relative to the theory have been identified, primarily in the measurements of $\overline{p_r}$ and $\delta_x p$. These vary with flow speed and incidence angle.

TABLE 2. Range of the BAT probe's systematic anomalies with flow speed and direction over the three speed classes and 25 set points of the wind tunnel test.

Parameter	Fast: 61 m s^{-1} (min, max) %	Medium: 51 (min, max) %	Slow: 36 (min, max) %
α	(−15, 8)	(−17, 6)	(−12, 11)
β	(−2, 14)	(−2, 7)	(−3, 12)
q as $\delta_x p$	(−4, 2)	(−7, 3)	(−2, 2)
p	(0.5, 0.7)	(0.6, 0.7)	(0.5, 0.6)
$\hat{u}_a$	(−2, 1)	(−2, 1)	(−1, 1)
$\hat{w}_a$	(−8, 15)	(−6, 16)	(−11, 12)

This test deals with mean equilibrium behavior. A dynamic-response test of the BAT probe and its instruments would require a measurable artificially generated disturbance in the incident flow or in the probe's orientation to it, a resource unavailable in this study.

a. Systematic anomalies

The measured mean anomalies in $\overline{p_r}$, $\delta_x p$, $\delta_y p$, and $\delta_z p$ represent small adjustments to the theory for the actual probe tested. These were propagated as deterministic linear perturbations on the theoretical equations to estimate the resultant anomaly in the derived velocity components $\hat{w}_a$, $\hat{u}_a$, and ultimately w itself. This provides a measure of the systematic error incurred using the optimized parameter values of section 7 without further adjustment, much as would be done using in-flight calibration only. Wind tunnel–related uncertainty in the anomaly estimates for $\hat{w}_a$ and $\hat{u}_a$ was estimated by bootstrap resampling, described later.

We start with the Mach number M, which is approximated within $O[(q/p)^2] \approx 0.04\%$ by

$$M^2 = \frac{2}{\gamma}\frac{q}{p}, \tag{8}$$

where $\gamma = 1.4$ is the ratio of the specific heat at constant pressure to the specific heat at constant volume. From anomalies p' and q', the resultant anomaly M' in the Mach number is estimated:

$$M^2\left(1+\frac{M'}{M}\right)^2 = \frac{2}{\gamma}\frac{q}{p}\left(1+\frac{q'}{q}\right)\left(1-\frac{p'}{p}\right). \tag{9}$$

Since these estimates involve measured systematic anomalies, the sign in the last factor of (9) is significant. From M and ambient temperature T, we obtain the true

airspeed U, the magnitude of the flow relative to the probe:

$$U = M(\gamma RT)^{1/2}. \tag{10}$$

With anomaly T' determine U' by

$$U\left(1+\frac{U'}{U}\right) = M(\gamma RT)^{1/2}\left(1+\frac{M'}{M}\right)\left(1+\frac{T'}{T}\right)^{1/2}. \tag{11}$$

The airspeed U is distributed over the probe coordinates' "horizontal" and "vertical" components, $\hat{u}_a$, $\hat{v}_a$, and $\hat{w}_a$ as

$$\begin{pmatrix} \hat{u}_a \\ \hat{v}_a \\ \hat{w}_a \end{pmatrix} = \frac{U}{D}\begin{pmatrix} -1 \\ \tan\beta \\ \tan\alpha \end{pmatrix},$$

$$D = (1 + \tan^2\beta + \tan^2\alpha)^{1/2}. \tag{12}$$

The cross component $\widehat{v_a}$ is not considered further. It has no effect on $\hat{w}_a$ if roll is zero, as in the current study. With anomalies α' and β', determine the denominator's anomaly D' from

$$D\left(1-\frac{D'}{D}\right) = (1 + \tan^2\beta + \tan^2\alpha)^{1/2} \times (1 - \beta'\tan\beta - \alpha'\tan\alpha), \tag{13}$$

leading to $\hat{u}'_a$ and $\hat{w}'_a$ through

$$\hat{u}_a\left(1+\frac{\hat{u}'_a}{\hat{u}_a}\right) = \frac{-U}{D}\left(1+\frac{U'}{U}\right)\left(1-\frac{D'}{D}\right),$$

$$\hat{w}_a\left(1+\frac{\hat{w}'_a}{\hat{w}_a}\right) = -\hat{u}_a\tan\alpha\left(1+\frac{\hat{u}'_a}{\hat{u}_a}\right)\left(1+\frac{\alpha'}{\tan\alpha}\right). \tag{14}$$

The WBWT measurements populate all foregoing anomaly terms. The wind relative to the probe has its earth-coordinate vertical component w_a given by

$$w_a = \hat{w}_a\cos\theta + \hat{u}_a\sin\theta, \tag{15}$$

where θ is the pitch angle. Roll is zero in these tests. The corresponding anomaly estimate, ignoring anomaly in θ, is

$$w_a\left(1+\frac{w'_a}{w_a}\right) = \hat{w}_a\left(1+\frac{\hat{w}'_a}{\hat{w}_a}\right)\cos\theta + \hat{u}_a\left(1+\frac{\hat{u}'_a}{\hat{u}_a}\right)\sin\theta. \tag{16}$$

Anomaly in θ is beyond the scope of the wind tunnel test, but for completeness we note its specified magnitude by high-quality GPS/INS to be within 0.1°. For U = 57 m s^{-1} and $\theta < 10°$, that translates to 0.1 m s^{-1}.

b. Statistical significance of systematic-anomaly field

Uncertainty in the measured systematic anomalies for q, α, and β might arise in a wind tunnel from several sources. For q there might be disparate measurement locations, different sample rates, dys-synchrony of measurements, long-term transients in the flowstream, and uncertainty in the BAT probe's orientation. The dynamic pressure in the wind tunnel was measured by a Pitot-static system located in the free stream near the roof at the immediate entrance to the test section. The BAT probe's q was measured in the center of the wind tunnel's cross section about 1 m into the test section. The ~1.5-m separation of measurement sites was judged to have minimal effect. The wind tunnel's design minimizes coherent spatial structures in the flow that might affect the two displaced sensors differently, with a possible exception noted in the next paragraph.

For anomalies of α and β the probe's orientation is the main source of uncertainty. The mount was sufficiently firm to eliminate any shifts of the probe's orientation. It was remotely controlled from outside the wind tunnel so that the flow was not interrupted between settings. Its rigidity maintained the yaw position during changes in pitch. Laser measurements at each new yaw setting, however, required opening a door to the outer pressure vessel enclosing the test section. Although the tunnel was not pressurized, small pressure differences generated a signal in both the BAT probe's and wind tunnel's sensors of q. The discrepancy between the two sensors' reports was unusually large during such events, and the data were not used. We speculate that a coherent disturbance was generated that affected the two sensors differently.

The static pressure is measured at four taps around the test section's elliptical perimeter (vertical plane) approximately coplanar with the mount at about 1.5 m into the test section. The signal is known to be noisy, but it is less than 2% relative to the mean. As discussed in section 6b, the probe's anomaly was uncertain, but small.

At each of the 75 set orientations of the probe, data were taken for at least 30 s. The BAT probe samples at 50 s^{-1}, while the wind tunnel samples at 2 s^{-1}, which constitutes at least 60 samples from the wind tunnel and 1500 samples from the BAT probe. These signals' frequency bands are matched using a low-pass four-pole Butterworth filter having a half-power point at 0.5 Hz.

This is below the Nyquist frequencies of the wind tunnel and the BAT probe by factors of 2 and 50, respectively. The filter is applied forward and backward to cancel the phase shift.

The samples' autocorrelation is estimated from the wind tunnel's time series of q, a measure of the regularity of the incoming flow. Since q depends on temperature, we used the q_{Ti} from (7), filtered as described above. The autocorrelation coefficient for q_{Ti} has a precipitous drop evident for the fast-speed class in Fig. 10. The center spike characterized the other two speed classes as well, but residual correlation remained after the drop, probably due to adjustments, starts, and stops made within the lower-speed classes. These produced slight step changes in speed, but not during the actual 30-s data runs. A time scale was derived by integrating the correlation out to 60 s of lag, by which time the integral had mostly flattened. It was less than 2.5 s for the fast speed. We estimate, therefore, 12 degrees of freedom in each sample.

Bootstrap resampling was used to provide confidence limits on anomaly estimates α', β', q', $\hat{u}'_a$, and $\hat{w}'_a$ for each attitude and speed setting. The autocorrelation, which reduces the degrees of freedom, was accounted by "moving block" bootstrap resampling (Wilks 1997; Efron and Tibshirani 1998).

The moving-block method collects not single data, but contiguous blocks of sufficient length, in this case 2.5 s (125 samples), that their means are uncorrelated. For convenience the wind tunnel's data were interpolated to 50 s^{-1}. Blocks were then drawn from the set of 1500 or more (autocorrelated) data at each setting with replacement and with any amount of overlap. These blocks, whose means are uncorrelated because of their random selection, were laid end to end without overlap thus preserving the original autocorrelation. Sufficient blocks were used to form a new sample of approximately the same total length as the original. As with ordinary bootstrap resampling, some of these drawings will cover the original series evenly, while others will favor one part of the original series over other parts. The 95% confidence intervals for the mean anomaly were derived from 1000 such drawings using the percentile method.

The range of individual systematic-anomaly components' estimates out to the 95% confidence limits is given in Table 2. Because of the singularity in (14), the systematic anomaly at $\alpha = 0$ is taken to be zero. This is justified in theory by (2) and (3) although $\delta_z p$ in Fig. 7 varies slightly with ψ (or β_S) for $\theta = 0$, and $\delta_y p$ with θ for $\psi = 0$. Such discrepancies are within the uncertainty of the measurements, but intolerable in the vicinity of the singularity. The anomaly range for p is computed relative to the wind tunnel's mean static pressure for each speed class.

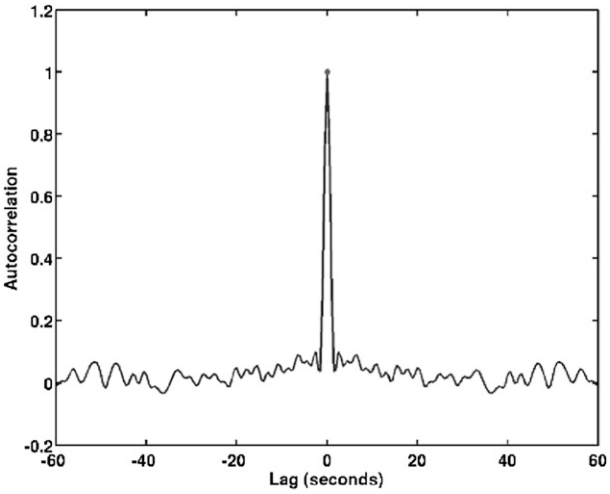

FIG. 10. Autocorrelation of temperature-independent dynamic pressure q_{Ti} measued by the wind tunnel's Pitot-static system for the fast-speed class, 62 m s^{-1}. The integral time scale is less than 2.5 s.

The confidence estimates also provide a significance test for the derived patterns of $\hat{u}'_a$ and $\hat{w}'_a$. By null hypothesis, the systematic anomalies $\hat{u}'_a$ and $\hat{w}'_a$ are constant over all α and β. The 95% confidence intervals for means of $\hat{u}'_a$ and $\hat{w}'_a$ at any one incidence angle α or β, however, only sometimes include the means realized at any other angles (Fig. 11). The systematic anomaly is clearly a significant function of the incidence angle. Curve fitting with respect to α and β on this particular probe will improve the accuracy. It is also possible to explore the contribution of these measured anomalies to fluxes derived from a more general BAT probe's measurements.

c. *Flux-anomaly estimate for a real case*

The effect of these anomalies on fluxes can be estimated by developing a time series of w'_a, the anomaly in w_a (earth coordinates) resulting from a real-world set of fluctuating sideslip, pitch, and attack angle over a pattern of known systematic anomaly. An expression for w'_a as a function of α, β, and θ can be readily obtained from (16).

Time series of α, β, and θ were obtained from turbulence measurements in flight in the boundary layer on 18 June 2005 over Illinois, when the Sky Arrow of the University of Alabama flew in the early morning under light turbulence and in the midmorning in strong turbulence (Kirby et al. 2008). The Sky Arrow's airspeed, 40 m s^{-1}, falls in the slow category of this paper. Flight altitude was 20 m AGL. This fairly typical case contains at least 250 s of contiguous data covering 10 km of air. The distance traveled over the ground depends on the wind and is not important to the argument.

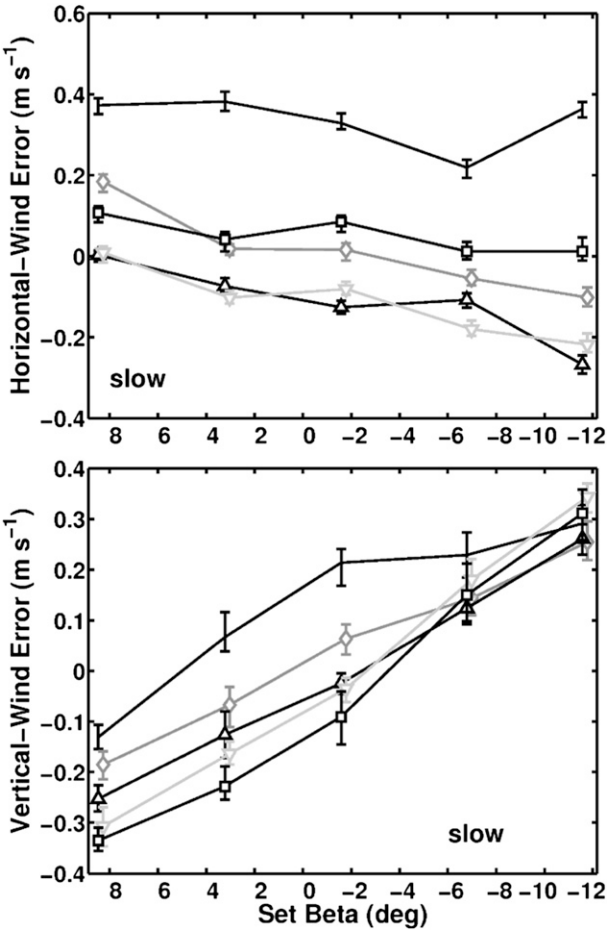

FIG. 11. Mean systematic anomaly (m s^{-1}) in the horizontal ($\hat{u}_a$) and vertical ($\hat{w}_a$) probe-coordinate components of wind in the slow-speed class as a function of β for the five settings of α: dark lines: high (10°, square), middle (0°, triangle Δ), low (−10°, no symbol). Gray lines: mid-up (5°, diamond), mid-down (−5°, triangle ∇). The 95% confidence interval is estimated by moving-block bootstrap. See the text.

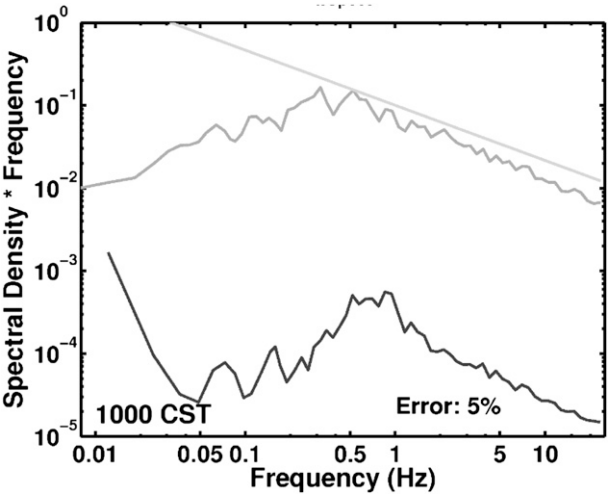

FIG. 12. Spectra of reported vertical wind (gray) and of the anomaly (black) estimated from the fluctuation of α and β over the BAT probe's fixed pattern of systematic anomaly. The straight line depicts the inertial subrange's theoretical decrease in frequency-weighted spectral density with the $-2/3$ power of the frequency. The incidence-angle data came from a flight in strong turbulence at 1000 central standard time (UTC − 6 h) on 18 Jun 2005 in rural Illinois.

Figures 12 and 13 characterize the anomaly w'_a (earth coordinates) resulting from the observed fluctuations of incidence angle over the pattern of systematic anomaly determined in the wind tunnel. The BAT probe used in this case is not the one tested in the wind tunnel. Additionally assumed is that the anomaly in w_a is the total anomaly in w. In fact, there are also anomalies, and random errors, in measurement of the airplane's motion and attitude and of the corrections for flow distortion (mostly upwash). The reported values of α, β, and θ, however, are accepted as a representative sample of convective boundary layer turbulence.

The spectra of both w, taken from the Illinois dataset, and w'_a from the current calculations, have similar shapes. The quantities are strongly correlated, as would be expected. The standard deviation of w'_a (determined by integrating the spectral density) is about 5% of that similarly determined for w. The effect on the reported CO_2 flux is a strong +20% in the early morning (Fig. 13, upper). The w'_a cospectrum is evidently correlated with that of w. The anomaly has more effect than would appear from the figure because at this time of minimal photosynthesis the negative and positive areas of the w-CO_2 cospectrum are partially cancelling. By mid-morning on the same day (Fig. 13, lower) the flux overestimation fell to within 1%, while the ratio of standard deviation of w remained about 5%.

9. Conclusions and recommendations

Three basic questions are addressed in this study.

(i) What are the characteristic anomalies of the BAT probe as tested?
(ii) What design changes appear to give the most promise of reducing these anomalies?
(iii) Can a generic anomaly characterization be made for BAT probes?

The BAT probe of this test, with such optimizations as are generally implemented through flight maneuvers, exhibited an overall systematic anomaly of about 10%–15% in the (true) vertical component of the wind relative to the probe, the component fundamental to

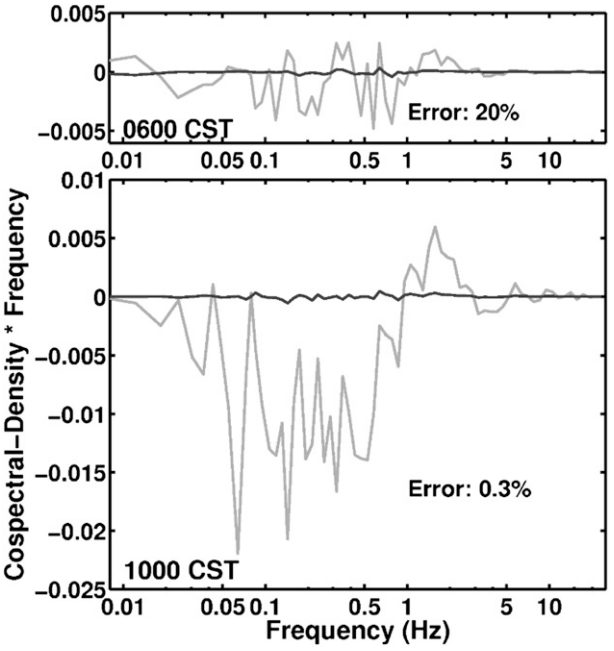

FIG. 13. Cospectrum of vertical wind with CO_2 (gray) from the flight of Fig. 12, along with the cospectrum of the estimated anomaly with the CO_2 mixing ratio (black). The spurious flux implied by correlation with the anomaly is +20% of the measured flux for the early-morning case in stable air before photosynthesis had started. By midmorning, the anomaly has dropped below 1%. The positive sign means the systematic anomaly w'_a produces an overestimate of the flux's magnitude.

boundary layer eddy correlation. Given an adequate GPS/INS to measure the velocity of the probe over the ground, this is quite acceptable for many purposes, as considerable field experience has shown.

A caution is raised by the finding of significant flow at nonzero angles of attack and sideslip through the tubing network linking the four reference ($\overline{p_r}$) ports. The data from our first wind tunnel visit were seriously corrupted by a kink in one of the tubes. The asymmetries still found in $\overline{p_r}$ and $\delta_x p$ absent the kink, appeared initially to reflect the tubes' influence, but this influence was found minimal. Nevertheless, a kink would be a disaster for a BAT probe in a field expedition. We emphasize the importance of checking the tubes. They must be as close as possible to the same length, and especially they must all have exactly the same diameter.

Having characterized this BAT probe's systematic anomaly, we can make some further analysis. We applied the anomaly structure of Fig. 11 to a case drawn from Sky Arrow flights over Illinois and found a 5% anomaly in the standard deviation of the vertical wind component relative to the probe both in light turbulence of early morning and strong turbulence of late morning. The effect on the weak early-morning CO_2 flux was a fairly sizeable 20%, which became a negligible 0.3% with late-morning photosynthesis. Being systematic, these anomalies, if known for a particular probe, are amenable to modeling and correcting. The degree of benefit can be assessed by repeating the calculations with the corrections applied.

Drawing on the findings of Garman et al. (2006) we placed the FUST 111 mm behind the BAT probe's head. With the FUST thus removed, we found no evident distortion of α, confirming their conclusion. Given this result, we can ask if our data provide generic characterization of BAT probes' anomaly. Two unexplained departures from theory militate against this. The dynamic pressure q is better represented by $\delta_x p$ alone than by (4), and α is better computed by the low-resolution scheme while β is better computed by the BAT scheme. It is unwise to apply these unexplained findings to a general BAT probe, although in-flight maneuvers may show them useful for particular systems.

In view of the expanding use of gust-probe systems for airborne measurement of turbulent fluxes, a proven generic design of characterized—and minimized—systematic anomaly is desirable. A review of the pressure sensors' characteristics, especially under vibration, is important. Also the adequacy of 16-bit A/D conversion and the extent of its degredation by aliasing should be reviewed. This work is in progress. The greatest improvement in accuracy, however, is likely to be through optimization of aerodynamic design. To this end we recommend another wind tunnel test to explain the unexpected behavior of $\delta_x p$ and $\overline{p_r}$. The test should include an idealized BAT probe, aerodynamically the cleanest possible, with all ports the same 1-mm diameter and with no fast-flow port or bypass flow. Necessary features, such as the FUST and the gas-sampling tubes, can then be added and their influence characterized.

This study has characterized an individual BAT probe configured for use with the Harvard ICOS sensors of CO_2 and CH_4. It also provides a new assessment of the expected uncertainly in airborne flux measurements and important insights to guide the design of a generic wind tunnel test.

Acknowledgments. The expert and good-spirited support of Richard Perdichizzi of the Aeronautics and Astronautics Department of MIT made the work at the Wright Brothers Wind Tunnel productive and enjoyable. Important improvements were suggested by Richard Eckman and an anonymous reviewer.

REFERENCES

Avissar, R., and Coauthors, 2009: The Duke University helicopter observation platform. *Bull. Amer. Meteor. Soc.,* **90,** 939–954.

Bange, J., T. Spieß, and A. van den Kroonenberg, 2007: Characteristics of the early-morning shallow convective boundary layer from Helipod flights during STINHO-2. *Theor. Appl. Climatol.,* **90,** 113–126, doi:10.1007/s00704-006-0272-2.

Beswick, K., M. Gallagher, A. Webb, E. Norton, and F. Perry, 2008: Application of the Aventech AIMMS20AQ airborne probe for turbulence measurements during the Convective Storm Initiation Project. *Atmos. Chem. Phys.,* **8,** 5449–5463.

Bögel, W., and R. Baumann, 1991: Test and calibration of the DLR Falcon wind measuring system by maneuvers. *J. Atmos. Oceanic Technol.,* **8,** 5–18.

Brown, E. N., C. A. Friehe, and D. H. Lenschow, 1983: The use of pressure fluctuations on the nose of an aircraft for measuring air motion. *J. Climate Appl. Meteor.,* **22,** 171–180.

Covert, E. E., cited 2004: A student's introduction to the Wright Brothers Wind Tunnel. Massachusetts Institute of Technology Tech. Rep., 20 pp. [Available online at http://web.mit.edu/aeroastro/labs/wbwt/student_wt_guide.pdf.]

Crawford, T. L., and R. J. Dobosy, 1992: A sensitive fast-response probe to measure turbulence and heat flux from any airplane. *Bound.-Layer Meteor.,* **59,** 257–278.

——, and ——, 1997: Pieces to a puzzle: Air-surface exchange and climate. *GPS World,* **8,** 32–39.

——, and ——, 2004: Accuracy and utility of aircraft flux measurements. *Vegetation, Water, Humans and the Climate: A New Perspective on an Interactive System,* P. Kabat et al., Eds., Springer Verlag, 566–571.

——, ——, and E. J. Dumas, 1996a: Aircraft wind measurement considering lift-induced upwash. *Bound.-Layer Meteor.,* **80,** 79–94.

——, ——, R. T. McMillen, C. A. Vogel, and B. B. Hicks, 1996b: Air-surface exchange measurement in heterogeneous regions: Extending tower observations with spatial structure observed from small aircraft. *Global Change Biol.,* **2,** 275–286.

Eckman, R., cited 1999: Computation of flow angles and dynamic pressure on a BAT Probe. Air Resources Laboratory, National Oceanic and Atmospheric Administration ARL/FRD Contribution, 4 pp. [Available online at http://www.noaa.inel.gov/Personnel/Eckman/docs/flowangles.pdf.]

Efron, B., and R. Tibshirani, 1998: *An Introduction to the Bootstrap.* CRC Press, 436 pp.

French, J. R., T. L. Crawford, R. C. Johnson, and O. R. Coté, 2001: A high-resolution temperature probe for airborne measurements. Preprints, *11th Symp. on Meteorological Observations and Instrumentation,* Albuquerque, NM, Amer. Meteor. Soc., 5.10. [Available online at https://ams.confex.com/ams/annual2001/webprogram/Paper17705.html.]

Garman, K. E., and Coauthors, 2006: An airborne and wind tunnel evaluation of a wind turbulence measurement system for aircraft-based flux measurements. *J. Atmos. Oceanic Technol.,* **23,** 1696–1708.

——, P. Wyss, M. Carlsen, J. Zimmerman, B. Stirm, T. Carney, R. Santini, and P. Shepson, 2008: The contribution of variability of lift-induced upwash to the uncertainty in vertical winds determined from an aircraft platform. *Bound.-Layer Meteor.,* **126,** 461–476, doi:10.1007/s10546-007-9237-y.

Gioli, B., and Coauthors, 2004: Comparison between tower and aircraft-based eddy covariance fluxes in five European regions. *Agric. For. Meteor.,* **127** (1–2), 1–16.

——, F. Miglietta, F. P. Vaccari, A. Zaldei, and B. De Martino, 2006: The Sky Arrow ERA, an innovative airborne platform to monitor mass, momentum and energy exchange of ecosystems. *Ann. Geophys.,* **49,** 109–116.

Hacker, J. M., and T. L. Crawford, 1999: The BAT-probe: The ultimate tool to measure turbulence from any kind of aircraft (or sailplane). *Tech. Soar.,* **23,** 42–45.

Hall, P. G., E. J. Dumas, and D. L. Senn, 2006: NOAA ARL mobile flux platform instrumentation integration on University Of Alabama Sky Arrow environmental aircraft. NOAA Air Resources Laboratory Tech. Memo. ARL-257, 41 pp. [Available online at http://aero.eng.ua.edu/equipment/noaa_tm.pdf.]

International Organization for Standardization, 1988: *ISO-1151: Flight Dynamics—Concepts, Quantities and Symbols—Part 1: Aircraft Motion Relative to the Air.* 4th ed. International Organization for Standardization, 29 pp.

Kalogiros, J. A., and Q. Wang, 2002: Calibration of a radome-differential GPS system on a Twin Otter research aircraft for turbulence measurements. *J. Atmos. Oceanic Technol.,* **19,** 159–171.

Kirby, S., R. Dobosy, D. Williamson, and E. Dumas, 2008: An aircraft-based analysis method for discerning individual fluxes in a heterogeneous agricultural landscape. *Agric. For. Meteor.,* **148,** 481–489.

LeMone, M., R. Grossman, F. Chen, K. Ikeda, and D. Yates, 2003: Choosing the averaging interval for comparison of observed and modeled fluxes along aircraft transects over a heterogeneous surface. *J. Hydrometeor.,* **4,** 179–195.

Lenschow, D. H., 1970: Airplane measurements of planetary boundary layer structure. *J. Appl. Meteor.,* **9,** 874–884.

——, 1986: Aircraft measurements in the boundary layer. *Probing the Atmospheric Boundary Layer,* D. H. Lenschow, Ed., Amer. Meteor. Soc., 39–55.

MacPherson, J., R. Grossman, and R. Kelly, 1992: Intercomparison results for FIFE flux aircraft. *J. Geophys. Res.,* **97** (D17), 18 499–18 514.

Neininger, B., W. Fuchs, M. Bäumle, A. Volz-Thomas, H. Prevot, and J. Dommen, 2001: A small aircraft for more than just ozone: Metair's Dimona after ten years of evolving developments. Preprints, *11th Symp. on Meteorological Observations and Instrumentation,* Albuquerque, NM, Amer. Meteor. Soc., 5.7. [Available online at https://ams.confex.com/ams/annual2001/webprogram/Paper18070.html.]

Sayres, D. S., and Coauthors, 2009: A new cavity based absorption instrument for detection of water isotopologues in the upper troposphere and lower stratosphere. *Rev. Sci. Instrum.,* **80,** 044102, doi:10.1063/1.3117349.

Traub, L. W., and O. Rediniotis, 2003: Analytic prediction of surface pressures over a hemisphere-cylinder at incidence. *J. Aircr.,* **40,** 645–652.

van den Kroonenberg, A., T. Martin, M. Buschmann, J. Bange, and P. Vörsmann, 2008: Measuring the wind vector using the autonomous mini aerial vehicle M^2AV. *J. Atmos. Oceanic Technol.,* **25,** 1969–1982.

Vellinga, O. S., B. Gioli, J. A. Elbers, A. A. M. Holtslag, P. Kabat, and R. W. A. Hutjes, 2010: Regional carbon dioxide and energy fluxes from airborne observations using flight-path segmentation based on landscape characteristics. *Biogeosciences,* **7,** 1307–1321, doi:10.5194/bg-7-1307-2010.

——, R. J. Dobosy, E. J. Dumas, B. Gioli, J. A. Elgers, and R. W. A. Hutjes, 2013: Calibration and quality assurance of flux observations from a small research aircraft. *J. Atmos. Oceanic Technol.,* **30,** 161–181.

Wilks, D., 1997: Resampling hypothesis tests for autocorrelated fields. *J. Climate,* **10,** 65–82.

Witinski, M., D. Sayres, and J. Anderson, 2011: High precision methane isotopologue ratio measurements at ambient mixing ratios using integrated cavity output spectroscopy. *Appl. Phys.,* **102B,** 375–380, doi:10.1007/s00340-010-3957-2.

Wroblewski, D., O. Coté, J. Hacker, and R. Dobosy, 2007: Cliff-ramp patterns and Kelvin–Helmholtz billows in stably stratified shear flow in the upper troposphere: Analysis of aircraft measurements. *J. Atmos. Sci.,* **64,** 2521–2539.

Zulueta, R. C., W. C. Oechel, H. W. Loescher, W. T. Lawrence, and K. T. Paw U, 2011: Aircraft-derived regional scale CO_2 fluxes from vegetated drained thaw-lake basins and interstitial tundra on the Arctic coastal plain of Alaska. *Global Change Biol.,* **17,** 2781–2802, doi:10.1111/j.1365-2486.2011.02433.x.